Society of Petroleum Engineers

SPE-182487-MS

Revisiting the Ideal Packing Theory with a Novel Particle Size Measurement Approach

A. Amer, B. Carter, E. Hudson II, H. Du, and C. Judd, Newpark Drilling Fluids

This paper was prepared for presentation at the SPE Asia Pacific Oil & Gas Conference and Exhibition held in Perth, Australia, 25-27 October 2016.

Abstract

Drilling into production zones requires the use of special fluids with minimal formation damage potential. These fluids typically include a blend of carefully designed bridging particles. The selection of these bridging particles is based on particle size distribution (PSD) and may include other attributes such as acid solubility depending on type of rock and the well completion method. One of the theories that addresses the design of these fluids is the Ideal Packing Theory (IPT).

Two of the most common ways to obtain PSD are laser diffraction (LD) and sieve analysis (SA). Each method has its own bias in measurement. For instance, SA tends to emphasize the second largest dimension of a particle (Kumar et al. 2013) while LD calculates PSD based on the assumption all particles are spheres. Particles in drilling fluids are not all spherical, therefore it was deemed worthwhile to investigate PSD measured by other techniques such dynamic imaging analysis (DIA) which takes in consideration the parameter aspect ratio when generating its PSD.

Sphericity of the bridging particles is a key assumption for the IPT to work. However, the use of dynamic image analysis (DIA) in the field of particle characterization in drilling fluids has led to significant findings. A key finding is that most bridging particles used are neither spherical nor uniform.

This study evaluates whether there are differences in the PSD results for the same sample of bridging particles. The study then examines the effect of using the data from the various PSD techniques on the bridging algorithm thus impacting the fluid sealing ability of porous media represented by ceramic disks.

This study also examines the phenomena of "packing behavior randomness" and its impact on porosity and permeability of blends of bridging particles.

Introduction

Theory and Modeling

In designing a reservoir drill-in fluid, it is critical that one of the primary design targets is minimal damage to the production zones. Aside from drilling operations, one of the mechanisms that may cause damage to the production zones comes from the drilling fluid. Invasion of solids from the mud into these zones can severely hinder production over the life of the well. Generally, a high filtrate loss is associated with higher

fluid and solids invasion causing more damage to the zone. The goal, therefore, is to be able to reduce filtration and seal off most, if not all, the pore throats until drilling operations are completed.

To limit the filtrate loss, it is essential that the drilling fluid generate a filtercake that can seal voids on the wellbore face. The first part of filtercake creation includes particles coming together, i.e., 'bridging', which promotes sealing. This is followed with more particles accumulation or 'packing' on and around these bridges which ultimately seals off the void. The dynamic nature of drilling operations results in many undetermined downhole parameters such as a vast array of porosity and permeability of geologic formations. Consequently, there are no explicit working equations to ensure the perfect seal. The industry must rely on a probabilistic approach in selecting the optimum sizes of these bridging particles.

Historically, several approaches have been developed to guide in the design of bridging particles. One well-known approach is Abram's rule (1977) which states that "the median particle size of the bridging material should be equal to or slightly greater than ⅓ the median pore size of the formation." (Dick et al. 2000). Additionally, the concentration of the sized particles should be in abundance of the solids concentration by at least 5% by volume. Though Abram's theory is simple and a good guide for the aspects of bridging, it does not deal with a secondary component of sealing the void, i.e., the packing aspect.

The Ideal Packing Theory (IPT) attempts to handle both components – bridging and packing – in several generalized guidelines. An ideal target line based off the porous characteristic of the media is also plotted on this graph, with one point typically being the median pore size, and the other being the origin point of the plot. In the absence of sufficient porosity data, median pore size is estimated as the square root of the permeability in milliDarcy (mD). According to IPT, ideal packing will occur if the material's particle size distribution (PSD) matches with the ideal target line. In practice, there is not a single material with a distribution that will match this linear target line, so material blends are often used. A linear line on a cumulative volume percent (CV%) vs d^x plot indicates that there will be an equal volume percentage of each particle size when referring to the bridging material or each pore size when referring to the porous medium. This is rather impractical, since neither the PSD of bridging particles nor the distribution of the pore throats sizes are linear.

Over the years, more studies been done to validate and improve on IPT. Kaeuffer (1973) simplifies the PSD of the bridging blend by setting the variable exponent (x) to 0.5. Chellapah and Aston (2012) found that adjusting the variable exponent, varying from 0.25 (for a particle distribution containing more fine sizes) to 1.25 (for a particle distribution containing coarse sizes), can lead to lower filtrate loss in certain scenarios.

Vickers (2006) optimized the target parameters of IPT by setting boundary conditions base on pore throat size distribution stating that "a large proportion of the production flow from a reservoir will come from the largest pore throats, thus these higher permeability/porosity zone must not be ignored." The target blend should meet the following standard:

- the blend's d_{90} is the largest pore throat size
- the blend's d_{75} is <⅔ of largest pore throat size
- the blend's d_{50} is between ±⅓ mean pore throat size
- the blend's d_{25} is around $^1/_7$ the mean pore throat size
- the blend's d_{10} is the smallest pore throat size

These works make the argument that IPT is not a one-size-fit-all solution, suggesting that fluid loss minimization requires consideration of both particle size and pore size distribution parameters. All these IPT systems heavily rely on the accuracy of the bridging material's PSD measurements.

Particle Size Analysis Techniques

Characterization of bridging agents via dynamic imaging analysis (DIA) promotes a comprehensive approach to quantifying multiple shape factors, thus subsequently providing insight as to why historical IPT approximations are contradictory when applied. Traditionally the assumption of spherical particle shapes has been at the forefront of calculations regarding IPT studies. This current study compares particle size analysis (PSA) data acquired using laser diffraction (LD), sieve analysis (SA) and DIA as building blocks in the design of bridging calcium carbonate ($CaCO_3$, CalCarb) blend for drilling fluids (Figure 1). Selection of an applicable technology is a vital aspect of properly acquiring particle size measurements. The aforementioned techniques are the most widely adopted techniques throughout the industry and each innately possess advantages and disadvantages over the other. Distinct characteristics such as size, shape, topology and morphology influence the accuracy and authenticity of results.

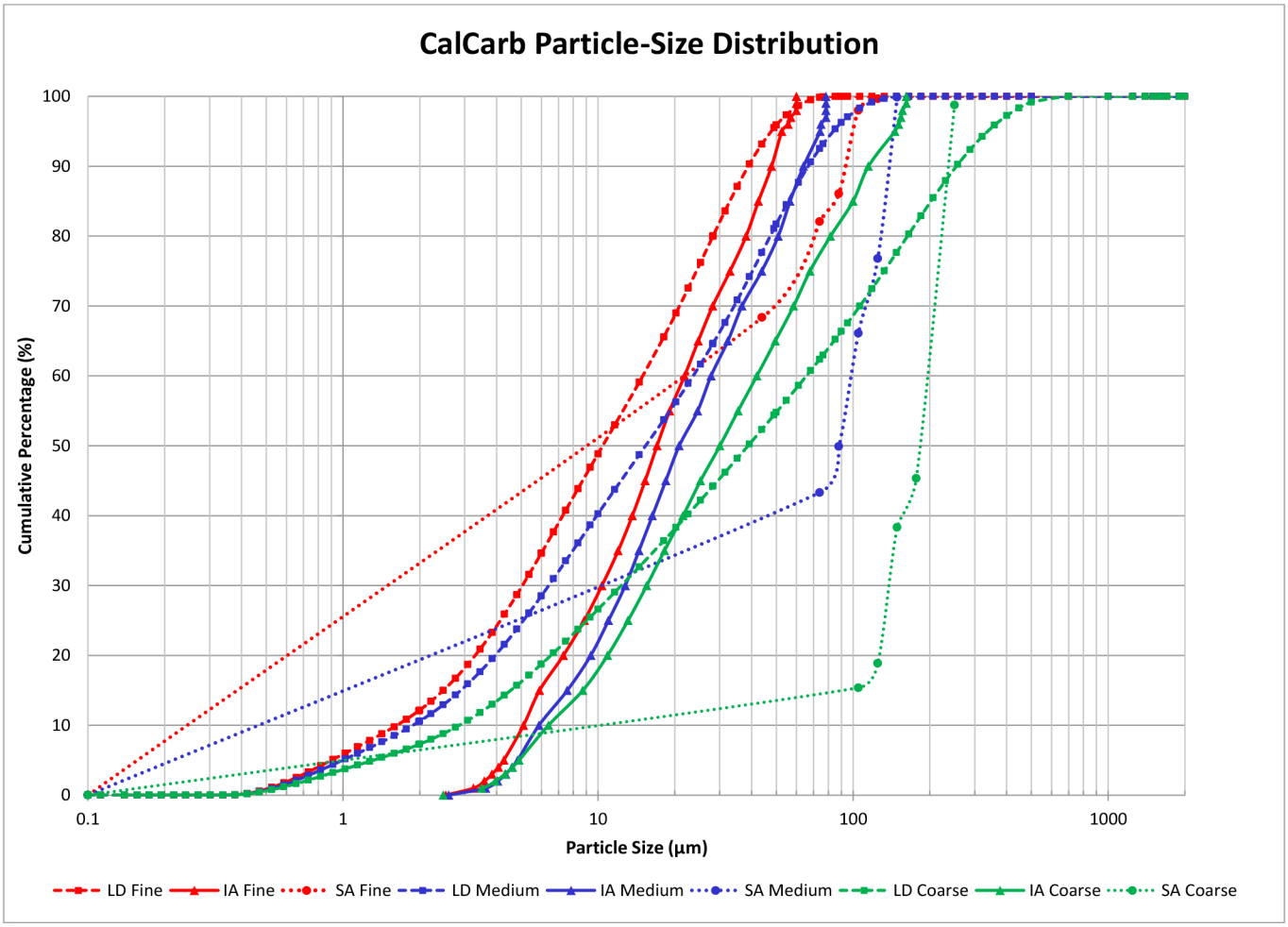

Figure 1—Particle Size Distribution using various PSA techniques.

Analysis of bridging solids is achieved traditionally via SA and LD. Due to the over-emphasis of the second largest dimension during SA, the PSD will not truly reflect genuine aspects of the particles dimensions. As the material vibrates on the screen, the particles orientate themselves optimally passing through the openings. As opposed to LD, SA provides a direct application to test for efficiency of bridging integrity, but may result in increased operator error given the physically demanding attributes of testing. A reduced resolution in data is apparent when compared to LD due to limitations of sieve screens sizes, with this effect being most noticeable when the d_{25} of the material is ≤44 µm.

LD investigates larger sample volumes than DIA over a broad dynamic range and provides a more precise measurement of smaller particles. Preliminary API recommendations suggest LD and DIA are the preferred method of testing for dry, isometric materials expected to have a d_{90} ≤1000 µm. The advantages of LD include: time-efficiency, non-destructiveness, and measurement repeatability (Virden 2010). Distribution calculations employ the Mie Scattering Theory (Rawle 2014) which forecasts the way light is scattered by particles that are spherical in nature. However, it does not apply to non-isometric particles. This exclusion of non-isometric particles leads to an inexact representation of the sample population using LD (Fluid Imaging Technologies 2015).

Contrary to the volumetric approach of LD and light scattering techniques, DIA interprets the morphological properties of each particle, not assuming all particles are spheres. DIA is a direct technique that provides detailed shape characteristic information of small sample sizes, but has analysis limitations of smaller micron size samples (Fluid Imaging Technologies 2015). For materials expected to have d_{25} >100 µm and very narrow particle size ranges (i.e., d_{90} to d_{10} <350 µm), DIA will be the preferred method, and SA methods will be considered as the less preferred alternative. Inclusion of shape factors like aspect ratio and circularity into the IPT equation could allow for the precise derivation of theoretical particle packing orientation, establishing a more explicit prescription of sized particulates assisting with bridging integrity. Subsequently, the application of shape factors via image analysis has the potential to maximize the bridging efficiency and minimize damage due to invasion.

Particle Size Distribution Testing

Dynamic Imaging Analysis

Dynamic particle imaging utilized digital images to measure size and shape characteristics of individual CalCarb particles sampled as per API standards (API RP 13B-1 2009). Homogenized 1-lb/bbl solutions of fine (F), medium (M) and coarse (C) CalCarb were blended at low shear rates and diluted to a final concentration of 5X with mineral oil. Measurements are taken using a FlowCam fluid imager with a 4X magnification lens using 300 and 600-µm flow cells. The CalCarb C sample was run using the larger size flow cell (600 µm) to avoid skewing the material's PSD by cutting off large particles from analysis. However, this comes at the price of reducing the morphological information available from small particles (under 12 µm) present in the solution. In the FlowCam, the sampled solution flows past the microscopes optics in the flow cell and thousands of particles are imaged per second. A strobed illumination source is employed in an effort to freeze the particles in motion synchronously with the cameras rapid shutter speed. Information collected included a variety of individual and statistical measurements related to the size and shape of particles for a comprehensive analysis of each sample (Figure 2).

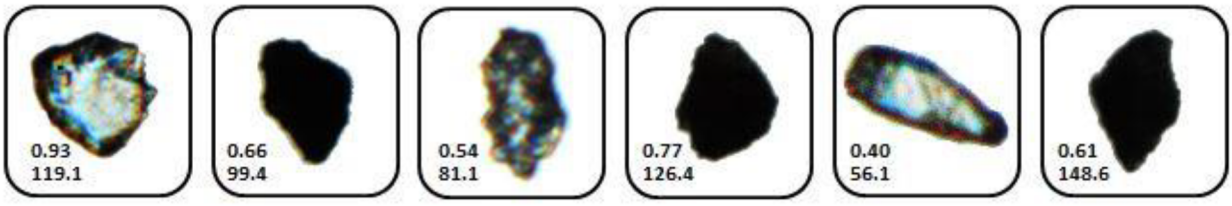

Figure 2—Dynamic Image Analyzer Data including aspect ratio and particle size values.

Particle Size Analysis by Laser Diffraction

Particle size imaging by LD was carried out using a Malvern Mastesizer 2000 equipped with a Hydro 2000G wet dispersion unit. Measurement of the PSD by LD was conducted by quantifying the angular aberrations in beam concentration passing through a homogenized particulate sample. Commercial bridging agents available in three size ranges were tested in triplicates and used for a comparative data analysis (Table 1).

Table 1—Sizing Technique Comparison of CalCarb F,M & C

Particle Size (µm)	Dynamic Image Analysis (DIA)	Laser Diffraction (LD)	Sieve Analysis (SA)
CalCarb Fine			
d_{10}	5.1	1.6	6.0
d_{50}	17.0	10.3	31.0
d_{90}	47.9	39.1	94.0
CalCarb Medium			
d_{10}	5.8	1.8	17.0
d_{50}	20.8	15.3	88.0
d_{90}	63.4	65.5	137.0
CalCarb Coarse			
d_{10}	6.4	2.8	68.0
d_{50}	30.1	36.6	185.0
d_{90}	114.8	234.8	237.0

Permeability Plugging Test (PPT)

To compare the effectiveness of the bridging theory calculations in a drilling fluid, permeability plugging tests (PPT) were performed on four unweighted drilling fluids that contained only fluid loss starch, viscosifier, pH control, and 50.0 lb/bbl of bridging CalCarb. This drilling fluid is similar to what would be recommended as a drill-in fluid, as it allows for tight fluid loss control and easy cleanup. The three limestone-based CalCarb sizes incorporated in the blends are identified in Tables 1 and 2 as CalCarb F, M, and C. Ceramic aloxite disks with a mean pore throat size of 5 µm (air) /12 µm (mercury)were used for comparison of fluids, each containing 50.0 lb/bbl of a single-sized CalCarb. An additional fluid was tested using disks with a larger pore throat size of 10 µm (air) /20 µm (mercury) for validation that the particle size blends used are adequate for sealing such pore throats. Specifications stated the disks have 850 mD and 3D mercury permeabilities, respectfully.

Table 2—Fluid Formulations for PPT Tests

Product	CalCarb C	CalCarb F	CalCarb 5/12 µm	Calcarb 10/20 µm
FluidLoss Starch, lb/bbl	6.0	6.0	6.0	6.0
Viscosifier, lb/bbl	0.5	0.5	0.5	0.5
pH Buffer, lb/bbl	0.5	0.5	0.5	0.5
CalCarb F, lb/bbl	-	50.0	7.5	7.5
CalCarb M, lb/bbl	-	-	36.5	-
CalCarb C, lb/bbl	50.0	-	6.0	42.5

Test drilling mud was formulated to closely resemble an actual fluid that would be used in reservoir applications. Fluid was hot rolled for 16 hours at 180°F prior use for the PPT. CalCarb 5/12 µm and Calcarb 10/20 µm contain a blend of commercially available calcium carbonate using the bridging theory calculations.

The test fluid was loaded into the PPT cell and a water-saturated aloxite disk placed on the outlet side of the PPT cylinder. The cell was assembled as instructed by the manufacturer and heated to 180°F. A differential pressure of 500 psi was maintained while the filtrate collected over a 30-minute period.

The resulting fluid loss values are given in Figure 3 showing the filtrate as volume produced over time. The fluids with the blended CalCarb sizes have lower fluid loss values than those of the fluids containing only single-sized CalCarb, demonstrating the effectiveness of blending the CalCarb sizes.

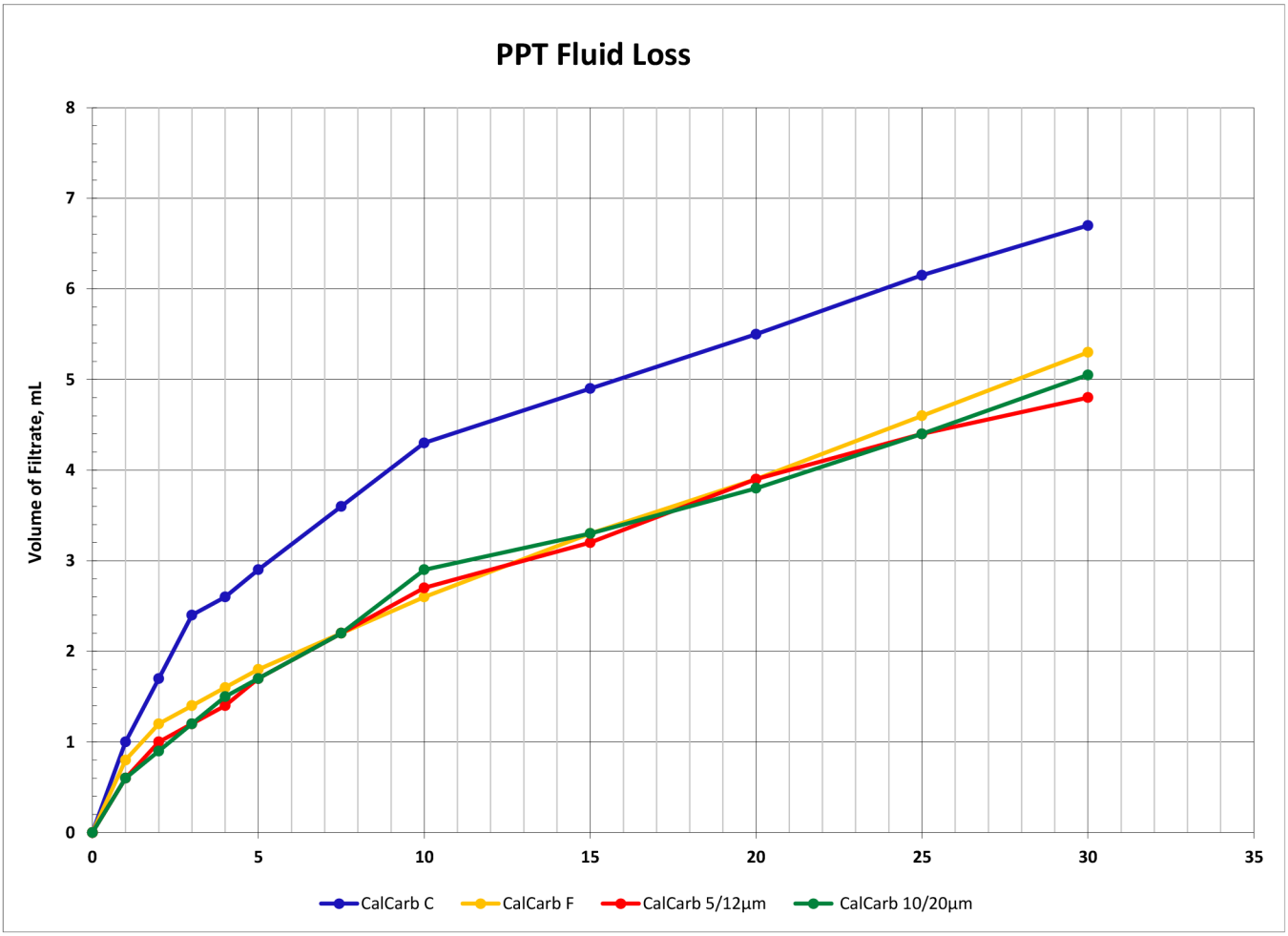

Figure 3—Comparison the PPT test results of all four fluids.

The bridging calculations in are adjusted to incorporate the PSA data acquired from DIA and LD (Tables 3 and 4). The CalCarb blend percentages were recalculated for the 5/12 µm and 10/20 µm disks using each set of particle size data. There is a notable difference in the bridging particle blends based on the product standard size and those of the analyzed calcium carbonate; however no laboratory tests have been performed to evaluate the recalculated blends.

Table 3—Particle Size Percentage

	Fine	**Medium**	**Coarse**
CalCarb 5/12 µm	15.0%	73.0%	12.0%
Calcarb 10/20 µm	15.0%	-	85.0%
DIA CalCarb 5/12 µm	No Solution	No Solution	No Solution
DIA CalCarb 10/20 µm	20.9%	79.1%	-
LD CalCarb 5/12 µm	91.1%	-	8.9%
LD CalCarb 10/20 µm	55.9%	-	44.1%

These blends are for both aloxite disk sizes used and calculated using the three parameters discussed during this study. The calculation is based on the "New Mercury" measurements of 12 and 20 µm. The DIA CalCarb 5/12 µm was not able to calculate a solution for the percentage to blend as the particle size did not meet the range required for a 12-µm pore throat size.

Table 4—Target vs. Results of Particle Size Calculated to Provide a Bridging Theory Solution

	d_{10} µm		d_{50} µm		d_{90} µm	
	Target, µm	Result, µm	Target, µm	Result, µm	Target, µm	Result, µm
CalCarb 5/12 µm	0.48	1.86	12.00	11.99	38.88	56.26
CalCarb 10/20 µm	0.80	2.17	20.00	19.70	64.80	132.55
DIA CalCarb 5/12 µm	-	-	-	-	-	-
DIA CalCarb 10/20 µm	0.80	5.70	20.00	20.00	64.80	60.41
LD CalCarb 5/12 µm	0.48	1.66	12.00	11.99	38.88	49.85
LD CalCarb 10/20 µm	0.80	2.06	20.00	20.01	64.80	105.15
A blend was not able to be calculated for the the DIA CalCarb 5/12 µm as the particle sizes did not meet the range required for a 12-µm pore throat size.						

Porosity/Permeability Measurements of Dry Bridging Particles Blends

The focus of this study was to measure the porosity and permeability of commercial limestone-based CalCarb F, M, and C to further evaluate the packing behavior of bridging particles. Previous studies have evaluated the effectiveness of bridging solids in filtercake and fluid-loss tests applications. While this does demonstrate how calculated PSD aids in forming a low-permeability filtercake, it does not address the packing tendencies of the CalCarb particles without the influence of liquids.

There are some challenges presented with measuring the porosity and permeability of ground CalCarb material. The bulk volume and surface area of the test material are necessary in the equation calculations for both porosity and permeability. The typical laboratory methods for obtaining bulk volume are geometric calculation or by fluid displacement. Fluid displacement is simply a volume measurement of the fluid displaced by the sample which, in our testing, would subsequently render the material unusable. In order to achieve a geometric bulk volume calculation of lose material, a sample cell is machined (Figure 6) wherein the inside of the container creates a right-faced cylinder. Fine mesh screens over the end openings allow for gas to flow through so that porosity and permeability data may be collected with minimum disturbance of the particles.

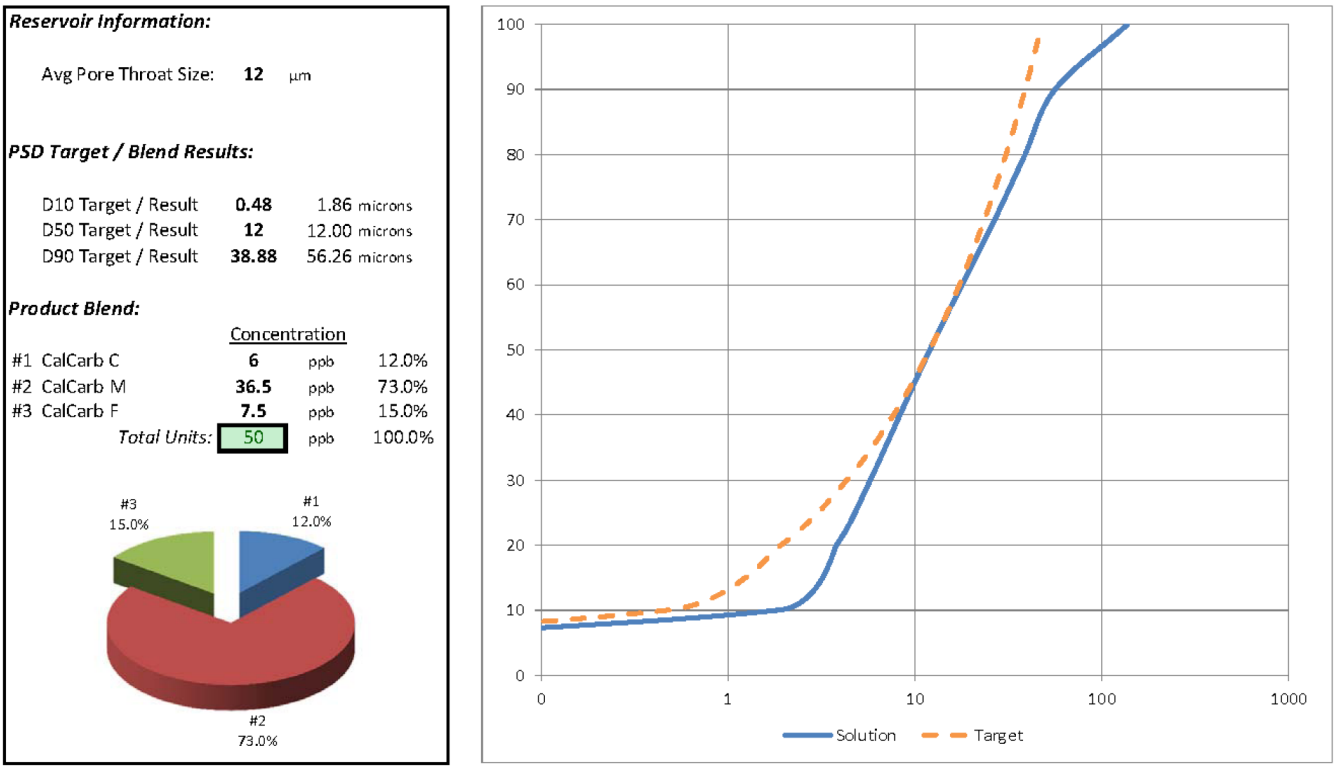

Figure 4—CalCarb blend based on bridging calculations of average pore throat size of 12 µm.

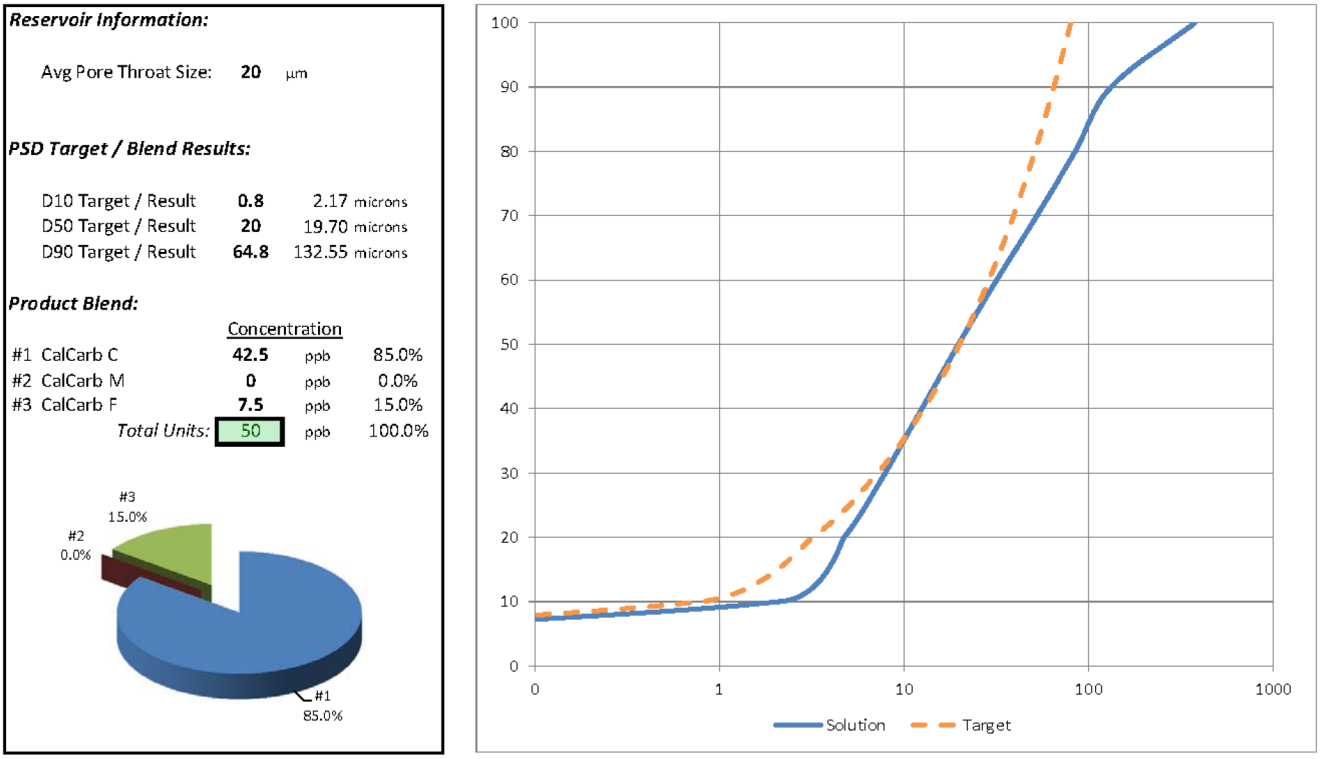

Figure 5—CalCarb blend on bridging calculations of average pore throat size of 20 µm.

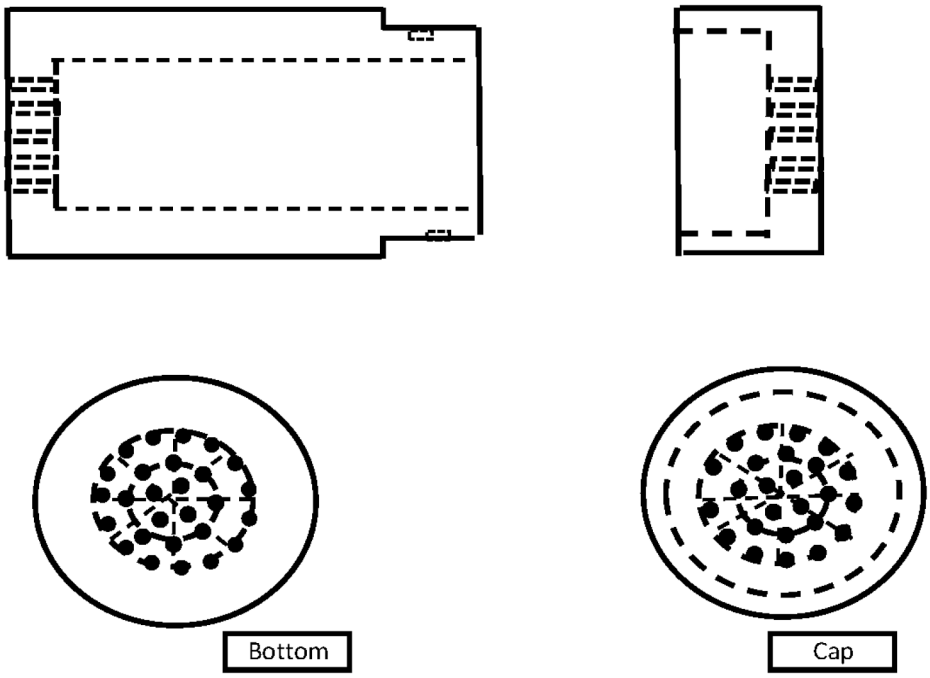

Figure 6—Bridging particles holding cell design.

Figure 7—Vinci Helium Porosimeter, Vinci (2013).

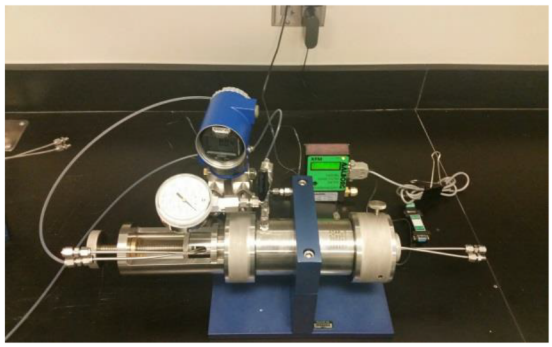

Figure 8—Phoenix Instruments Hassler-type coreholder for measuring gas permeability.

Porosity of the CalCarb along with samples blended according to bridging theory calculations for 5/12-μm and 10/20-μm ceramic aloxite disks were measured using a helium porosimeter. This equipment (Figure 10) utilizes Boyle's Gas Law (API RP 40 1998) to measure the grain volume of a sample which was then used to calculate porosity and pore volume using the following equations:

PV = Pore volume = voided space that can be filled by gas
ϕ = Porosity
BV = Bulk volume = calculated from sample diameter and length
GV = Grain volume = measured volume of solid particles in a sample
PV = BV – GV
ϕ = PV/BV

Prior to lab testing, the sample cell was required to be calibrated as a "billet" so that a correction could be made to account for the bulk volume the cell took up inside the sample cup. The weight of the dry CalCarb was recorded to calculate the grain density by dividing the sample weight by the measured grain volume (V_{grain}). The density for the samples in this test calculated in the 2.7 to 2.72 range, as expected for CalCarb. This verifies that the sample cell had been correctly adjusted for in the calculations. The helium porosimeter has a known calibrated volume (V_{ref}) that was pressured to 200 ±15 psi (P_{ref}). Once stable, the helium was then expanded into the sample chamber and the pressure drop recorded as (P_{exp}). This data was then used in the equations below for calculating grain volume under isothermal conditions per Vinci (2013).

V_{grain} = Volume of solid particles in a sample
P_{ref} = Reference Pressure (initial pressure)
P_{exp} = Expanded Pressure (final pressure)
V_{ref} = Determine during calibration using metal billets
V_{matrix} = Determine during calibration using metal billets

$$V_{grain} = \left(V_{matrix} + V_{ref}\right) - \frac{P_{ref}}{P_{\exp}} \times V_{ref}$$

Air permeability data was gathered on each of the samples after the porosity data was completed. The sample cell was removed from the porosimeter (Figure 11) and placed into a Hassler-type core cell with minimum agitation. By doing so, the porosity data could be correlated to its respective gas permeability. The sample cell has a rigid construction so that when confining pressure is applied, the loosely packed CalCarb is not compressed. Both outlets of the core holder were connected to a pressure differential meter that displayed the pressure drop as nitrogen was flowed through the sample. For gas permeability, a mass flow meter was necessary to record the flow rates of the nitrogen on the outlet side of the sample. For liquid permeability, it would be necessary to record the volume of liquid produced over a recorded time. The equation for calculating permeability is achieved by rearranging the terms from Darcy's Law:

$$K_g = 245 \times \frac{L}{A} \times \left(\frac{Q}{P_1 - P_2}\right) \times \mu$$

Where:
Kg = Gas permeability (mD)
L = Sample length (cm)
A = Area (cm^2)
Q = Flow rate (mL/min)
P_1 - P_2 = Pressure drop across the sample (psi)
μ = Dynamic viscosity (cP)

To determine the porosity and permeability of the CalCarb sizes and blends, material was loaded into the cell and lightly tapped to settle particles until no further material could fit. This allowed the bulk volume to remain constant and the variations depended on how many particles would fit into the sample cell. Repeats of each sample were tested to measure the porosity of the material if only approximately 37 grams filled the cell. This weight was chosen because 37 grams is the maximum CalCarb F material that would fit into

the cell. This makes the bulk volume and weight a constant value, allowing the grain volume and porosity to be the variations in test parameters. An alternative to this is to reduce the mass of material added evenly across all of the samples.

The porosity data collected in Table 5 agrees Chellappah's and Aston's (2012) and Bo et al. (1965) conclusion that a wider distribution of particle sizes results in a reduction in porosity. However, the grain volume increased with the size of the PSD in the samples that were filled to a loose packing. This test result is contrary to Challappah's conclusion that the packing density increases as the particle size is more linear. Results of the permeability testing were inconclusive due to the wide variations in results. This may be a factor of the packing randomness rather than test error or failure as the porosity measurements were consistent for each measurement.

Table 5—Porosity and Permeability Data

Sample name	Average Air Perm, (mD)	Bulk Vol (ml)	Dry Weight (g)	Grain Vol. (ml)	Grain density (g/ml)	Porosity (%)
CalCarb F	294	30.20	37.58	13.81	2.72	54.3%
CalCarb F, constant wt.	77.0	30.20	37.02	13.65	2.71	54.8%
CalCarb F constant wt. 2	78.6	30.20	37.35	13.75	2.72	54.5%
CalCarb M	619	30.20	38.29	14.14	2.71	53.2%
CalCarb M constant wt.	175	30.20	37.35	13.75	2.72	54.5%
CalCarb M constant wt. 2	298	30.20	37.52	13.80	2.72	54.3%
Calcarb C repeat	101	30.20	44.26	16.39	2.70	45.7%
Calcarb C constant wt.	203	30.20	37.00	13.65	2.71	54.8%
Calcarb C constant wt. 2	484	30.20	37.44	13.79	2.72	54.3%
CalCarb 5/12µm Random	168	30.20	38.29	14.14	2.71	53.2%
CalCarb 5/12µm Layered	112	30.20	38.14	14.06	2.71	53.4%
CalCarb 10/20µm Random	207	30.20	37.52	13.80	2.72	54.3%
CalCarb 10/20µm Layered	144	30.20	44.09	16.32	2.70	46.0%
CalCarb 10/20µm Layered, constant wt.	346	30.20	38.10	14.04	2.71	53.5%

Cumulative results of the porosity and permeability measurements on dry calcium carbonate. Results support the conclusion that as the PSD widens, the porosity decreases and the grain volume increases. The permeability of the material was not consistently repeatable which may be a factor of the random packing tendency of the particles.

Summary & Conclusion

- Dynamic Image Analysis, while useful in other characterization aspects, does not appear to offer an advantage over other PSA techniques for input data for IPT modeling.
- Testing confirmed the industry practice that broad PSD blends performed better than narrow PSD blends at PPT testing.
- A new test method (porosity/permeability measurement) was developed to study the packing structure behavior randomness.
- Preliminary testing indicates that the packing structure behavior randomness affects mainly permeability but not porosity.

Acknowledgements

The authors wish to thank Newpark Drilling Fluids for allowing the publication of this paper, Kent A. Peterson of Fluid Imaging Technologies for the loan of the flow cells required for testing, and Fred Growcock of the API PSA RP workgroup for guidance in regards to the proposed recommendations. The authors also extend gratitude to Newpark's technology group, with special thanks to Rick Jones for assisting in the design and manufacturing of the porosity and permeability cell and Antoine Thuriere and Greg Perez for technical guidance and editorial review.

Nomenclature

5/12 µm *: pore throat measurements of ceramic filter discs with air (5µm) and mercury, (12µm)*

10/20 µm *: pore throat measurements of ceramic filter discs with air (10µm) and mercury, (20µm)*

BoyBoyle's Gas Law *: the inverse relationship between pressure (P) and volume (V) of a quantity of an ideal gas at a constant temperature ($P_1V_1=P_2V_2$)*

BulBulk volume *: sample volume calculated from diameter and length.*

CalCalCarb *: the abbreviated term for Calcium Carbonate ($CaCO3_3$) used in this study.*

DarDarcy's Law *: the relationship that describes fluid flow through a porous medium*

d^x *: the particle diameter raised to an exponent which between the values of zero and one*

Grain volume *: in volume: the volume of solid particles in a sample.*

Pore Volumee *: the connected void space that can be filled by gas.*

Porosity *: the ratio of pore volume to bulk volume*

SI Metric Conversion Factors

lb/bbl x 2.853	E+00 = kg/m3
cP x 1.0	E-03 = Pa.s
psi x 6.894	E-03 = MPa

References

Abrams, A. 1977. "Mud Design to Minimize Rock Impairment Due to Particle Invasion." *SPE 5713-PA Journal of Petroleum Technology*, **v. 29**, no. 5 (May) 586–592. http://dx.doi.org/10.2118/5713-PA

Andreasen, A. M. and Andersen, J. 1930. "Relation between grain size and interstitial space in products of unconsolidated granules." *Kolloid-Zeitschrift*, vol. **50**, no. 3, 217–228.

API. 1998. *API RP 40 - Recommended Practices for Core Analysis*, 2nd edition, Washington, DC: API.

API. 2009. *API RP 13B-1 - Recommended Practice for the Field Testing of Water-Based Drilling Fluids, Annex F: Sampling, inspection and rejection, 2009*, Washington DC: API.

API. 2016. *API SG13 - TG4/WG3 - Size Analysis of Particulates in Drilling Fluids*, Washington DC: API.

Bo M. K., Freshwater D. C. and Scarlett B. 1965. "The Effect of Particle Size Distribution on the Permeability of Filter Cakes." *Chem. Eng. Res. Des*. Vol. **43a**, 228–232.

Chellappah, K. and Aston, M. 2012. "A New Outlook on the Ideal Packing Theory for Bridging Solids. SPE 151636, *SPE International Symposium on Formation Damage Control*, Lafayette, Louisiana, 15–17 February. http://dx.doi.org/10.2118/151636-MS

Dick, M. A., Heinz, T. J., Svoboda, C. F., and Aston, M. 2000. "Optimizing the Selection of Bridging Particles for Reservoir Drilling Fluids." SPE 58793, *SPE International Symposium on Formation Damage Control*, Lafayette, Louisiana, 23–24 February. http://dx.doi.org/10.2118/58793-MS

Fluid Imaging Technologies, Inc. 2015. *The Ultimate Guide to Dynamic Imaging Analysis*. Scarborough, ME: Fluid Imaging Technologies, Inc. http://info.fluidimaging.com/imaging-particle-analysis

Growcock, F. 2016. *Private Communication*. Houston, TX.

Horiba Instruments, Inc. 2014. *A Guidebook to Particle Size Analysis*. Irvine, CA: Horiba Instruments, Inc. https://www.horiba.com/fileadmin/uploads/Scientific/Documents/PSA/PSA_Guidebook.pdf

Kaeuffer, M. 1973. "Determination de L'Optimum de Remplissage Granulometrique et Quelques Proprieties S'y Rattachant." Congres International de I'A.F.T.P.V., Rouen, Oct.

Kaeuffer, M., Determination de L'Optimum deRemplissage Granulometrique et Quelques proprieties S'y Rattachant,: *presented at Congres International de I'A.F.T.P.v., Rouen, Oct*. 1973

Kaeuffer, M., Determination de L'Optimum deRemplissage Granulometrique et Quelques proprieties S'y Rattachant,: *presented at Congres International de I'A.F.T.P.v., Rouen, Oct*. 1973

Kumar, A., Chellapah, K., Aston M. and Bullgachev, R. 2013. "Quality Control of Particle Size Distributions." SPE 165150, SPE European Formation Damage Conference, Noordwijk, The Netherlands, 5-7 June. http://dx.doi.org/10.2118/165150-MS

Kumar, A., Savari, S., Whitfill, D. and Jamison, D. E. 2010. "Wellbore Strengthening: The Less-Studied Properties of Lost-Circulation Materials. SPE 133484, SPE Annual Technical Conference, Florence, Italy, 19-22 September. http://dx.doi.org/10.2118/133484-MS

OFITE. 2015. Permeability Plugging Tester Instruction Manual Vs 5.0. Houston, Texas.

Rawle, A. 2014. *Basic Principles of Particle Size Analysis*. Malvern, Worcestershire: Malvern Instruments Limited. https://www.researchgate.net/file.PostFileLoader.html?id=512f819ce39d5e7734000006&assetKey=AS%3A273632960417813%401442250590500

Vickers S., Cowie M., Jones T., Twynam A. 2006. "A New Methodology that Surpasses Current Bridging Theories to Efficiently Seal a Varied Pore Throat Distribution as Found in Natural Reservoir Formations. AADE-06-DF-HO-16, AADE Fluids Conference, Houston, Texas, 11-12 April. Available from www.AADE.org

VINCI Technologies. 2013. *Operating Manual and Maintenance Manual V3.20. Helium Porosimeter Educational for Grain Vol. using Matrix Cup*. France.

Virden, A. 2010. Method Development for Laser-Diffraction Particle-Size Analysis. Malvern, Worcestershire: Malvern Instruments Limited.